Anisotropic thermoelectric effect on phosphorene and bismuthene: First-principles calculations based on nonequilibrium Green's function theory

メタデータ	言語: eng
	出版者:
	公開日: 2022-02-18
	キーワード (Ja):
	キーワード (En):
	作成者:
	メールアドレス:
	所属:
URL	https://doi.org/10.24517/00065296

Anisotropic thermoelectric effect on phosphorene and bismuthene: First-principles calculations based on the non-equilibrium Green's function theory

Yuto Tanaka[1], Mineo Saito[2] and Fumiyuki Ishii[2] E-mail:

y-tanaka@cphys.s.kanazawa-u.ac.jp

[1]*Graduate School of Natural Science and Technology, Kanazawa University*

[2]*Division of Mathematical and Physical Science, Graduate School of Natural Science and Technology,*

Kanazawa University, Kakuma-machi, Kanazawa 920-1192, Japan

By using the non-equilibrium Green's function (NEGF) method, we perform first-principles calculations on phosphorene and bismuthene and evaluate the thermoelectric properties based on the Landauer formalism. We find figures of merit strongly depend on the transport direction: the figures for the zigzag (ZZ) direction are substantially different from those for the armchair direction. These anisotropies are found to originate from the difference between the transmission functions in the AM and ZZ directions. We find that p-type bismuthene has a large figure of merit when the transport is in the ZZ direction, then conclude that bismuthene has some advantage over phosphorene as a thermoelectric material. We also clarify that the spin-orbit coupling has substantial effect on thermoelectric properties in bismuthene.

1. Introduction

The thermoelectric materials, which can convert heat energy to electric energy, have attracted great interests due to the energy issue. To achieve high performance thermoelectric conversion, we need high values of the electric conductivity and the Seebeck coefficient and low values of thermal conductivities due to electron and phonon. Low dimensional and nanostructured materials could be new candidates for efficient thermoelectric conversion.[1–3] The power factor could be enhanced due to localized density of states near the Fermi energy and also the lattice thermal conductivity can be reduced by increase of phonon scattering. Furthermore quantum effects play an important role in nanostructures, where the length of the system is shorter than the mean-free-path. The non-equilibrium Green's function (NEGF) method is suitable for investigating the transport properties of such nanostructured systems; the efficiency of the thermoelectric conversion is represented by figure of merit ZT,

$$ZT = \frac{GS^2}{\kappa_{\mathrm{e}} + \kappa_{\mathrm{p}}} T, \tag{1}$$

where T, G, S and $\kappa_{\mathrm{e(p)}}$, respectively, denote the temperature, the electric conductance, the Seebeck coefficient and the thermal conductance due to electron (phonon).

Recently, phosphorene, which is the two dimensional material of phosphorus, is found to be a promising thermoelectric material. The figure of merit was found to be higher than

that of black phosphorous bulk.[4] Due to the anisotropy in electrical conductivity and lattice thermal conductivity[4–12,26], the thermoelectric performance in phosphorene is expected to be improved by selecting the transport direction. Furthermore, the figure of merit was found to be raised by applying strain;[7] this strain can be introduced by using substrates that vary the lattice constants.

The thermoelectric properties of other two-dimensional group V materials (arsenene, antimonene and bismuthene) have also been investigated; it is found that these materials are promising candidates for the thermoelectric conversion since those have high power factors and low thermal conductivities.[7,13,14] Here we focus on bismuthene, which is the {012} bilayer of bismuth and has a geometry similar to that of phosphorene. It is well known that the bulk bismuth has a low thermal conductivity compared with black phosphorous since the atomic mass of bismuth is much larger than that of phosphorous. Bismuthene is thus expected to have good thermoelectric properties. Indeed the figure of merit was predicted to be 0.8 from first-principles calculations without including spin-orbit coupling (SOC).[13] It is noted that bismuthene can be fabricated on some substrates. For example, it can be formed on the Si(111) and highly oriented pyrolytic graphite (HOPG) surface.[15–17] Bismuthene is affected by substrates and the magnitude of the effect depends on the substrates. In the case of bismuthene on Si(111) substrate, rugged wetting layers are constructed on the Si(111) surface and the substrate is expected to have little effect on electronic properties; thus the substrate is expected to be little effect on thermoelectric properties.[15,16] Bismuthene is found to be a semiconductor in the theoretical previous work[18,19] and thus is expected to be suitable for thermoelectric materials.

The aim of this paper is to compare the thermoelectric properties of phosphorene and bismuthene. In particular, we clarify the origin of the anisotropy in thermoelectric properties of both materials. We perform first-principles calculations by using the NEGF method and evaluate the thermoelectric properties in the zigzag (ZZ) and armchair (AM) directions based on the Landauer formalism. On the basis of our calculated results, we suggest that bismuthene has some advantage in thermoelectric properties over phosphorene and the anisotropy is expected to originate from the number of the channels in each direction transport. Since bismuth is a heavy atom, we include the SOC in the above calculations. We find that the SOC has an substantial effect on the thermoelectric effect.

2. Computational model

Fig. 1 shows the transport models of phosphorene and bismuthene in the zigzag direction, which are used in the NEGF calculations; in these calculations, we use a localized basis set. We consider the periodic system under zero bias voltage and divide into left and right regimes and expanded channel.[20] The expanded channel consists of the channel and the edges of left and right leads and the self-consistent electronic charge of the expanded channel is obtained by using the NEGF method; we assume that the electronic charge of the remaining parts (left- and right-regimes) are the same as that of the bulk. We define an extended unit cell and consider only the overlaps of localized basis orbitals in the same or neighboring cells in Fig. 1. The length of the extended unit cell in the transport direction is twice larger than the original unit cell where the lattice constants are a_{ZZ} and a_{AM}. In Fig. 1, we show the case of transport in the zigzag direction; the green dotted frames indicate the extended unit cell. Details of the Green's function-method-based calculation model was described in a previous study.[20]

3. Computational method

To evaluate thermoelectric properties of nanostructures, we use the Green's function method. The Green's function theory is based on the formalism of $\vec{k}$-resolved transmission function $\zeta^{(\vec{k})}(E)$ over the energy E as follows,[20]

$$\zeta^{(\vec{k})}(E) \quad = \quad \mathrm{Tr}\left[G_C^{(\vec{k})}(X)\Gamma_L^{(\vec{k})}(E)G_C^{\dagger(\vec{k})}(X)\Gamma_R^{(\vec{k})}(E)\right], \tag{2}$$

where the suffixes C, L and R indicate the channel, left-regime and right-one, respectively. $G_C^{(\vec{k})}$, $\Sigma_{L(R)}^{(\vec{k})}$ and $\Gamma_{L(R)}^{(\vec{k})}(E)$ are the retarded Green's function of the expanded channel, the self-energy and the spectral density function caused by coupling left (right)-regime and expanded channel, respectively. The complex energy X is given by $X = E + i\delta$, where δ is a positive infinitesimal. The transmission function $\zeta(E)$ of the expanded channel connected to the regimes is given by the Brillouin zone integration of $\zeta^{(\vec{k})}(E)$.

By using Eq. (2), the quantities, G, S and κ_e can be evaluated as follows[13)21)]:

$$G \quad = \quad eK_0, \tag{3}$$

$$S \quad = \quad -\frac{1}{eT}\frac{K_1}{K_0}, \tag{4}$$

and

$$\kappa_e \quad = \quad \frac{1}{eT}\left(K_2 - \frac{K_1^2}{K_0}\right), \tag{5}$$

where K_0, K_1 and K_2 are given by

$$K_{n=0,1,2} \equiv \frac{e}{h} \int \zeta(E)(E-\mu)^n \left(\frac{\partial f}{\partial E}\right) dE. \tag{6}$$

e, h, μ, T and f, respectively, represent the elementary charge, the Plank constant, the chemical potential, the temperature in the channel and the Fermi distribution function. We evaluate these quantities as a function of chemical potential μ based on the rigid band approximation.

The geometry and the electronic band structures are determined by using OpenMX code[22] based on the local density approximation (LDA) within the density functional theory (DFT). We use the norm-conserving pseudopotentials and pseudo atomic orbital (PAO) base as a localized base. In the cell-optimization, the PAO basis functions are specified by P7.0-$s3p3d2f1$ and Bi8.0-$s3p3d2f1$; in the case of the P (Bi) atom, we use the cutoff radius of 7.0 (8.0) in bohr unit and the pseudo basis function consisting of three s, three p, two d and one f atomic orbitals.[22] We next carry out the NEGF calculations to determine thermoelectric-electronic properties, The PAO basis functions used in these calculations are specified by P7.0-$s3p3d2$ and Bi8.0-$s3p3d2$. Whereas we carry out scalar-relativistic calculations on phosphorene, we use fully-relativistic calculations on bismuthene because the spin-orbit interaction is strong in the case of the bismuth atom. The atomic positions are optimized until the atomic force is less than 1.0×10^{-4} hartree/bohr.
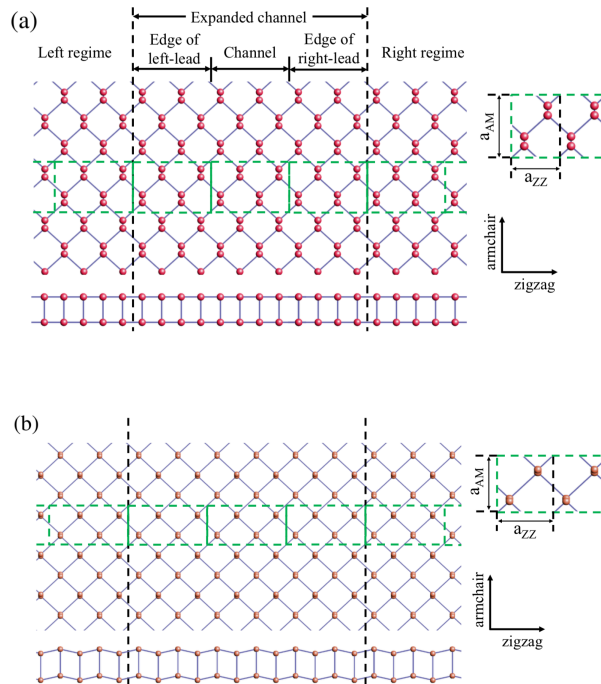
Fig. 1. Computational models of (a) phosphorene and (b) bismuthene from the top and side views. We show the transport model in the zigzag direction as example. The green dotted frame indicates the extended unit cell.

We first carry out the electronic band structure DFT calculations and obtain the self-consistent electronic charges. The obtained charge is used for describing the charge in the left- and right regimes. We use the k points of $8(16) \times 16(8) \times 1$ in calculating zigzag (armchair) direction transport. Then, we calculate transmission function by using the Green function method. We take the 64 k-point sampling for the direction which is perpendicular to the transport direction in Fig. 1.

4. Results and Discussion

We first optimize both primitive cell size and the atomic positions. In the cell-size optimization, we determined a_{ZZ} and a_{AM} (see Fig. 1 and Table I). The optimized bond lengths and the bond angles are shown in Fig. 2 and tabulated in Table I. Bismuthene is found to be buckled as was reported in a previous work[18]; the buckling amplitude Δz is estimated to be 0.5 Å. Phosphorene is found not to be buckled (see Table I).

Fig. 2.   Geometries of (a) phosphorene and (b) bismuthene.

Table I.   Geometric parameters of phosphorene and bismuthene

/	Phosphorene	Bismuthene
a_{ZZ}	3.28	4.50
a_{AM}	4.31	4.61
l_1 (Å)	2.23	3.08
l_2 (Å)	2.21	3.11
θ_1 (deg)	101.6	102.0
θ_2 (deg)	101.6	83.5
θ_3 (deg)	96.9	92.8
Δz (Å)	0.0	0.5

We next calculate the band structures (Fig. 3) and find that phosphorene is a semiconductor having the band gap of 0.62 eV (Fig. 3 (a)) whereas bismuthene with spin-orbit coupling

(SOC) (Fig.3 (b)) is a semiconductor having the band gap of 0.18 eV. The difference between electronic properties of phosphorene and bismuthene is expected to originate from the fact that in bismuthene, the s orbital is strongly localized and thus the sp hybridization is weakened as was discussed in a previous study.[18] Furthermore, we find that the SOC has a substantial effect on the band structure of bismuthene. As Fig.3 (c) shows, the band structure obtained from non-SOC calculation is different from that obtained from the SOC calculation. Therefore the SOC calculation is necessary to study bismuthene.

We next calculate the transmission function $\zeta(E)$ and find prominent anisotropies (Fig. 4). In phosphorene, $\zeta(E)$ in the AM direction is larger than that in the ZZ direction in the energy ranges of the valence and conduction bands. This trend is in a good agreement with that reported in previous study with NEGF method in tight-binding model.[5] In bismuthene, we find a substantial difference between the transmission function $\zeta(E)$ evaluated from the SOC and non-SOC calculations. Because of this difference, the thermoelectric properties are affected by the SOC as mentioned later.

The above mentioned anisotropies are expected to originate from the difference in the number of channels between the two directions. To demonstrate this, we here take an example of the transmission function at the Γ point $\zeta^{(\vec{k}=0)}(E)$ (Fig. 3). In the case of phosphorene, the number of channels in the ZZ (Γ-X) direction and AM (Γ-Y) direction are 2 and 6, respectively, at the energy which is 0.3 eV lower than the valence band top (see green dotted line in Fig. 3 (a)). This difference in the number of channels leads to the fact that $\zeta^{(0)}(E)$ in the AM direction is larger than that in the ZZ direction at that energy (Fig. 3 (a)). Meanwhile $\zeta^{(0)}(E)$ in the ZZ direction is larger than that in the AM direction at the energy which is 0.3 eV higher than the conduction band bottom (see purple dotted line in Fig. 3 (a)) since the number of channels (6) in the ZZ direction is larger than that (2) in the AM direction (Fig. 3 (b)). These differences in the number of the channels are expected to be the origin of the anisotropy in the transmission function $\zeta^{(\vec{k}=0)}(E)$.

In the case of bismuthene, the numbers of channels in the ZZ and AM directions are 0 and 4, respectively, at the energy which is 0.1 eV lower than the valence band top (see green dotted line in Fig. 3 (b)). The difference in the number of channels is the reason for the fact that $\zeta^{(0)}(E)$ in the AM direction is larger than that in the ZZ direction at the energy. On the other hand, the numbers of channels in the ZZ and AM directions are 4 at the energy which is 0.2 higher than the conduction band bottom (see purple dotted line in Fig. 3 (b)). This same number of the channels is expected to be the origin of the fact that $\zeta^{(0)}(E)$ in the AM direction is nearly equal to that in the ZZ direction at the energy. We furthermore calculate

the transmission function $\zeta^{(0)}(E)$ of bismuthene without including the SOC and investigate the influence of the SOC (Fig. 3 (c)). Since the electronic structure of bismuthene is different between SOC and non-SOC calculations, $\zeta^{(\vec{k}=0)}(E)$ is also affected by SOC.
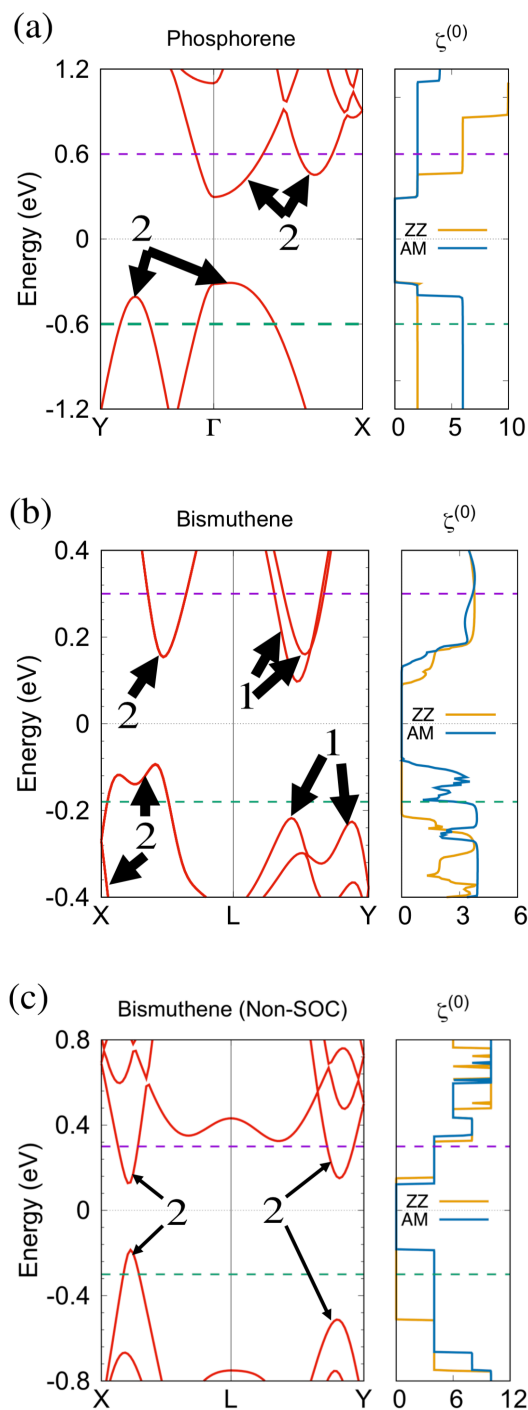
Fig. 3. Band structures and transmission function of (a) phosphorene, (b) bismuthene and (c) bismuthene without including SOC at Γ point. The degeneracies of the bands are indicated in the figure.
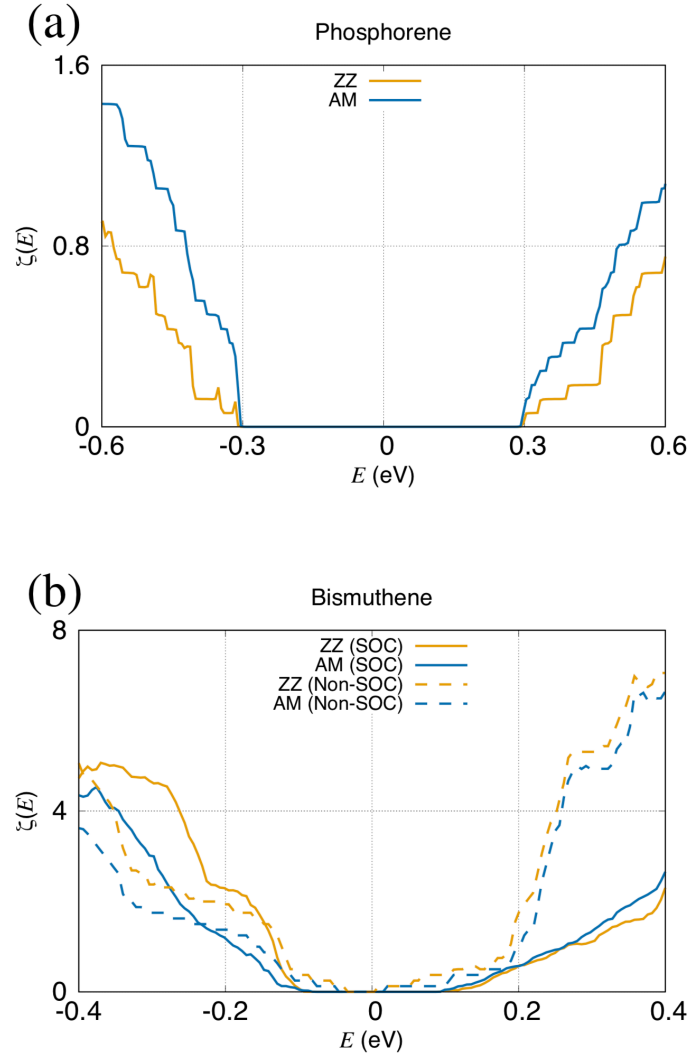
Fig. 4.   Transmission function $\zeta(E)$ in the direction of zigzag (ZZ) and armchair (AM): (a) phosphorene and (b) bismuthene.

As mentioned above, we demonstrate that the anisotropy of $\zeta^{(0)}(E)$ is explained based on the number of channels. Therefore, the anisotropy of $\zeta(E)$, which is obtained by integrating $\zeta^{(\vec{k})}(E)$ in the Brillouin zone, is also expected to be explained by considering the number of the channel in the Brillouin zone.

We next perform calculations for thermoelectric properties at 100 K and 300 K by using Eqs. (3)-(6). Fig. 5 (a) and Fig. 6 (a) show the electric conductance G of phosphorene and bismuthene, respectively, where $G_0 \equiv e^2/h$ is the quantized unit of electric conductance. We find that the electric conductance is insensitive to the temperature (100 K and 300 K). In phosphorene, the electric conductance in the AM direction is found to be larger than that in the ZZ direction. This difference is due to the fact that the transmission function in the AM direction is larger than that in the ZZ direction (Fig. 4 (a)). In bismuthene, the electric conductance in
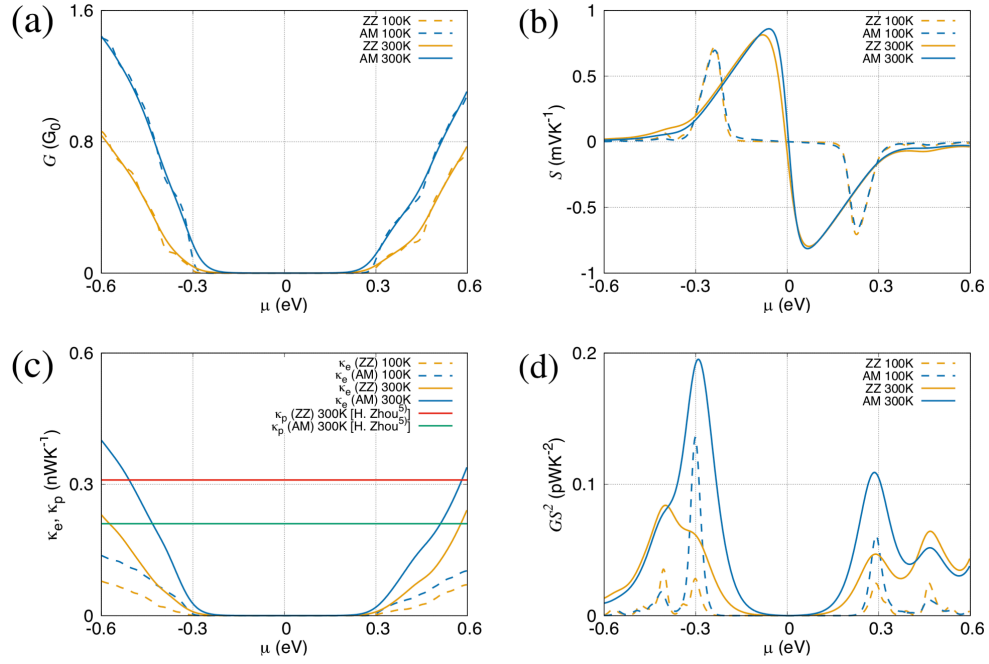
Fig. 5. Chemical potential dependence of thermoelectric properties in the direction of zigzag (ZZ) and armchair (AM) at 100 and 300 K: (a) Electric conductance, (b) Seebeck coefficient, (c) thermal conductance and (d) power factor of phosphorene.

the ZZ direction is found to be larger than that in the AM direction in the energy range of the valence band. This difference is due to the difference in the transmission function as in the case of phosphorene; the transmission function in the ZZ direction is larger than that in the AM direction (Fig. 4 (b)). The electric conductance for the conduction band energy range is not sensitive to the transport direction, which is due to the fact that the transmission function is also insensitive to the transport direction.

We next calculate the Seebeck coefficient S of phosphorene and bismuthene (Figs. 5 (b) and 6 (b)) and find that the coefficient depends on the temperature and the anisotropy in the transport direction is found to be small. On the other hand, the calculated electron thermal conductance κ_e is found to show some anisotropies (Fig. 5 (c) and Fig. 6 (c)); In the case of phosphorene, the values in the AM direction are larger than those in the ZZ direction. Meanwhile, in the case of bismuthene, the values in the ZZ direction are larger than those in the AM direction in the valence band energy range whereas the anisotropy is weak in the conduction band energy range. The above mentioned anisotropies in the thermal conductance are similar to those in the transmission functions. As mentioned above, transmission function, electric conductance and electron thermal conductance have similar anisotropies whereas the Seebeck coefficients have no strong anisotropy.
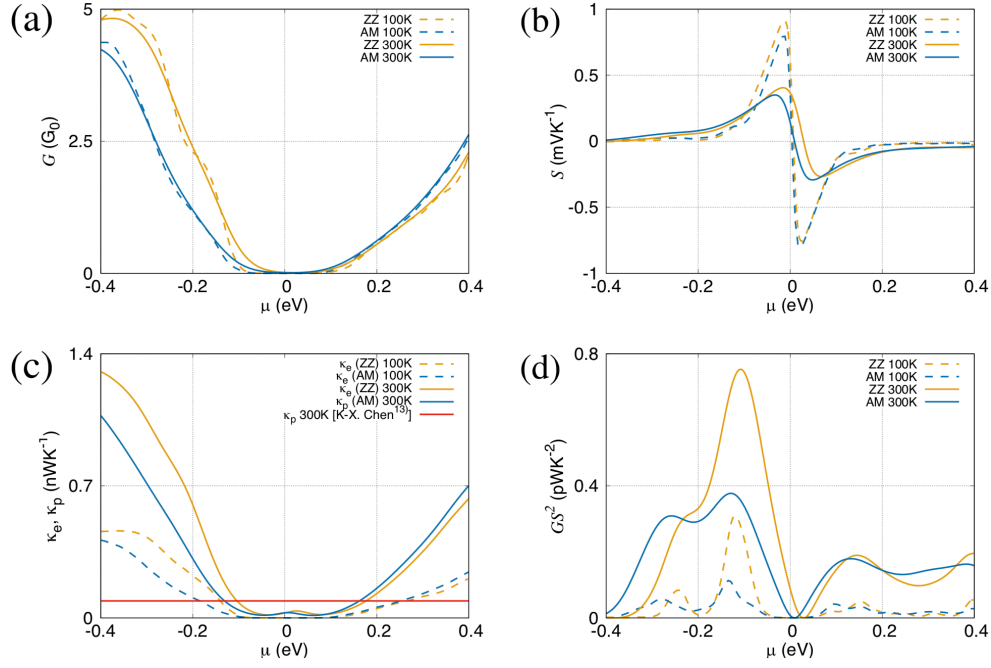
Fig. 6. Chemical potential dependence of thermoelectric properties in the direction of zigzag (ZZ) and armchair(AM) at 100 and 300 K: (a) Electric conductance, (b) Seebeck coefficient, (c) thermal conductance and (d) power factor of bismuthene.

We here estimate the power factor GS^2 from the results of the electric conductance G and the Seebeck coefficient S (Fig. 5(d) and 6(d)). The power factors of both phosphorene and bismuthene have an anisotropies similar to those in G near the band edge due to the fact that the anisotropy of S is very weak (Fig. 5). As a result, the anisotropy of power factor originates from transmission function since the anisotropy in the transmission function induces the anisotropy in G. The peak value of bismuthene in the ZZ direction (0.75 pWK^{-2}) is about 4 times larger than that of phosphorene in the AM direction (0.19 pWK^{-2}) at 300 K. This fact suggests that bismuthene has some advantage in power factor over phosphorene.

Finally, we estimate the figure of merit ZT at 300 K by using Eq. (1). The values of GS^2 and κ_e (Fig. 5 and 6) have been already calculated as mentioned above. As for the phonon thermal conductances κ_p at 300 K in phosphorene, we deduce the value of 0.31 (0.21) nWK^{-1} in the ZZ (AM) direction from the results of a previous calculation[5] (Fig. 5 (c)) ; the reported value was 1.08 (0.76) nWK^{-1}nm^{-2} in the ZZ (AM) direction. As Fig. 7(a) shows, the values of ZT in the AM direction is found to be larger than that in the ZZ direction. Here we discuss the origin of these characteristic features of ZT in phosphorene. In the denominator in Eq. (1), κ_p is much larger than κ_e (electron one) near the valence (conduction) band top (bottom). Since κ_p in the AM direction is smaller than that in the ZZ direction, the denominator contributes to

the fact that ZT in the AM direction is larger than that in the ZZ direction. As was mentioned above, GS^2 in the AM direction is larger than that in the ZZ direction, which also contributes to the anisotropy of ZT. We conclude that both numerator and denominator in Eq. (1) induces the anisotropy, i.e., ZT in the AM direction is larger than that in the ZZ direction.

For the phonon thermal conductances κ_p at 300 K in bismuthene, we deduce the value of 0.09 nWK^{-1} in both ZZ and AM directions from the results of a previous calculation[13] (Fig. 6 (c)) ; the reported values were 0.11 GWK^{-1}m^{-2} in both ZZ and AM directions. We find that the calculated ZT in the ZZ direction is larger than that in the AM direction when the Fermi energy (electron chemical potential) is near the valence band edge (Fig. 7(b)). On the other hand, when the Fermi energy is near the conduction band edge, ZT in the ZZ direction is close to that in the AM direction. We discuss the origin of these characteristic features of ZT in bismuthene. Both κ_p and κ_e contribute to the denominator in Eq (1) near the edge of band. In the energy region near the edge of valence band, the denominator is almost isotropic since the anisotropies of κ_e and κ_p are weak. Therefore the anisotropy of ZT in this energy region mainly originates from the numerator in Eq (1), ZT in the ZZ direction is larger than that in the AM direction since GS^2 in the ZZ direction is larger than that in the AM direction. In the energy region near the edge of conduction band, ZT have weak anisotropy since the anisotropies of both numerator and denominator in Eq. (1) are weak. To evaluate the anisotropy in bismuthene exactly, we need to calculate the values of κ_p in both ZZ and AM directions but this is beyond of the scope of this study.

We also estimate ZT of bismuthene by using the non-SOC calculation, and clarify that the SOC has large effect on ZT as shown in Fig. 7(b). The peak values are enhanced by the SOC. The peaks of ZT estimated by including (excluding) SOC are 1.47 (0.53) and 0.77 (0.62) in the ZZ and AM directions respectively.

We find that ZT in the p-type bismuthene is larger than that in the n-type bismuthene and is larger than those in p- and n-type phosphorene (see Fig. 6). We tabulate the peak value of ZT for the phosphorene, bismuthene and bi(111) monolayer. Since the peak value of bismuthene is larger than that in phosphorene, we suggest that bismuthene is a good candidate for a thermoelectric material.

5. Conclusions

We carried out first-principles calculations on thermoelectric properties of phosphorene and bismuthene by using the NEGF method. We found the anisotropic thermoelectric properties of phosphorene and the bismuthene and have clarified the origin of the difference. We

Table II. Peak value of ZT in the ZZ and AM direction at 300 K.

/	ZZ	AM	Other works
Phosphorene	0.07	0.26	$0.22^{5)[a]}$, $0.05^{7)[a]}$, $0.33^{8)[a]}$, $0.14^{26)[a]}$
Bismuthene	1.47	0.77	$0.75^{13)[b]}$
Bi(111) monolayer	-	-	$0.62^{23)[b]}$, $2.4^{24)[c]}$, $1.75^{13)[d]}$

[a]: *p*-type in the AM direction

[b]: *p*-type in the ZZ direction

[c]: *n*-type Bi(111) monolayer in some direction

[d]: *p*-type Bi(111) monolayer in some direction
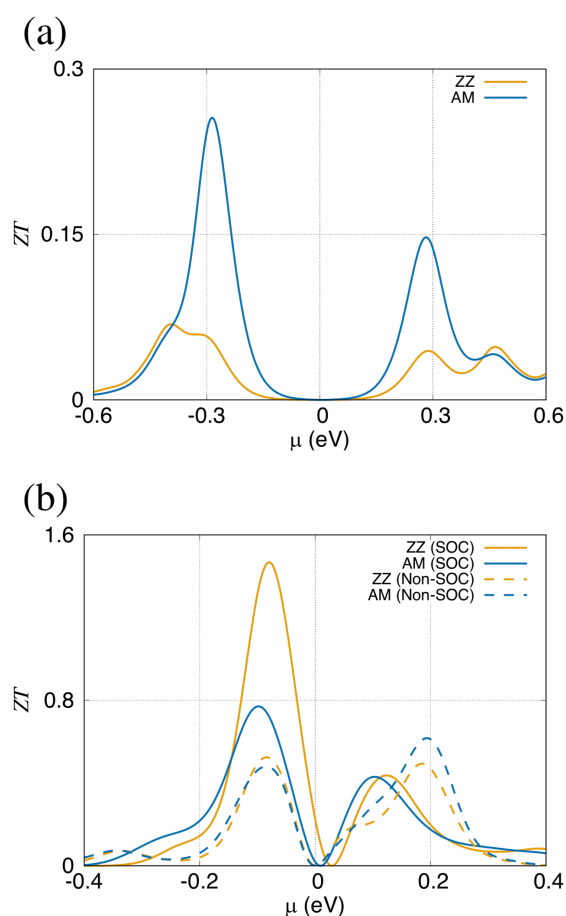
Fig. 7. Chemical potential dependence of figure of merit ZT at 300 K in the zigzag (ZZ) and armchair(AM) directions: (a) phosphorene and (b) bismuthene.

first found some anisotropy in the transmission function $\zeta(E)$. Then we found that the electric conductance G has an anisotropy similar to $\zeta(E)$ whereas the Seebeck coefficient S has no strong anisotropy. As a result, the power factor GS^2 has similar anisotropy to that in $\zeta(E)$. We furthermore clarified that ZT has anisotropy similar to that in GS^2. In bismuthene, we include the SOC effect in our calculations and clarify that the SOC has substantial effect on ZT. We

conclude that p-type bismuthene in the ZZ direction has a large value of ZT, suggesting that bismuthene is a strong candidates for thermoelectric material.

Acknowledgment

References

1) L. D. Hicks, M. S. Dresselhaus: Phys. Rev. B **47**, 12727 (1993).

2) L. D. Hicks, M. S. Dresselhaus: Phys. Rev. B **47**, 16631 (1993).

3) M. S. Dresselhaus, G. Chen, M. Y. Tang, R. Yang, H. Lee, D. Wang, Z. Ren, J-P. Fleurial, and P. Gogna: Adv. Mater. **19**, 1043 (2007).

4) H. Y. Lv, W. J. Lu, D. F. Shao, and Y. P. Sun: arXiv:1404.5171.

5) H. Zhou, Y. Cai, G. Zhang and Y. W. Zhang: J. Mater. Res. **31**, 20, (2016) 3179-3186.

6) R. Fei, A. Faghaninia, R. Soklaski, J-A. Yan, C. Lo, and L. Yang: Nano Lett. **14**, 6393 (2014).

7) H. Y . Lv, W. J. Lu, D. F. Shao, and Y. P. Sun: Phys. Rev. B **90**, 085433 (2014).

8) L. M. Sandonas, D. Teich, R. Gutierrez, T. Lorenz, A. Pecchia, G. Seifert, and G. Cuniberti: J. Phys. Chem. C **120**, 18841 (2016).

9) Z-Y. Ong, Y. Cai, G. Zhang, and Y-W. Zhang: J. Phys. Chem. C **118**, 25272 (2014).

10) M. Zare, B. Z. Rameshti, F. G. Ghamsari, and R. Asgari: Phys. Rev. B. **95**, 045422 (2017).

11) A. Jain, and AJH. McGaughey: Sci. Reports **5**, 8501 (2015).

12) G. Qin, Z. Zhang, SY. Yue, Z. Qin, H. Wang, Y. Han, and M. Hu: Phys. Rev. B. **94**, 165445 (2016).

13) K-X. Chen, S-S. Lyu, X-M. Wang, Y-X. Fu, Y. Heng, and D-C. Mo: J. Phys. Chem. C **121**, 13035 (2017).

14) Y. Sun, and Z. Shuai: J. Phys. Chem. C **121**, 19080 (2017).

15) T. Nagao J. T. Sadowski, M. Saito, S. Yaginuma, Y. Fujikawa, T. Kogure, T. Ohno, Y. Hasegawa, S. Hasegawa, and T. Sakurai: Phys. Rev. Lett. **93**, 105501 (2004).

16) S. Yaginuma, T. Nagao, J. Sadowski, M. Saito, K. Nagaoka, Y. Fujikawa, T. Sakurai, T. Nakayama: Surf. Sci. **601**, 3593 (2007).

17) S.A.Scott, M. V. Kral, and S. A. Brown: Surf. Sci. **587**, 175 (2005)

18) M. Saito, Y. Takemori, T. Hashi, T. Nagao, and S. Yaginuma: Jpn. Appl. Phys. **46**, 7824 (2007).

19) E. Aktürk, O. Üzengi. Aktürk, and S. Ciraci: Phys. Rev. B. **94**, 0144115 (2016).

20) T. Ozaki, K. Nishio and H. Kino: Phys. Rev. B. **81**, 035116 (2010).

21) D.Hayashi, Y. Nakai, H. Kyakuno, T. Yamamoto, Y. Miyata, K. Yanagi and Y. Maniwa: Appl. Phys. Express **9**, 125103 (2016).

22) T. Ozaki et al.: Open source package for Material eXplorer,

http://www.openmx-square.org/

23) D. C. Zhang, A. Zhang, S. Guo, Y. Duan: RSC Adv., **7**, 24537 (2017)

24) L. Cheng, H. Liu, X. Tan, J. Zhang, J. Wei, H. Lv, and J. Shi: J. Phys. Chem. C **118**, 904 (2014).

25) G. Qin, Q. Yan, S. Yue, M. Hu, and G. Su: Phys. Chem. Chem. Phys **17**, 4854 (2014).

26) B. Lioa, J. Zhou, B. Qiu, M. S. Dresselhaus, and G. Chen: Phys. Rev. B. **91**, 235419 (2015).